ACS APPLIED MATERIALS & INTERFACES

Research Article

www.acsami.org

Diaminohexane-Assisted Preparation of Coral-like, Poly(benzoxazine)-Based Porous Carbons for Electrochemical Energy Storage

Shuai Wang, Ling Zhang, Fei Han, Wen-Cui Li, Yuan-Yuan Xu, Wen-Hui Qu, and An-Hui Lu*

State Key Laboratory of Fine Chemicals, School of Chemical Engineering, Dalian University of Technology, Dalian 116024, People's Republic of China

Supporting Information

ABSTRACT: The assembly of commercial silica colloids in the presence of 1,6-diaminohexane and their subsequent encapsulation by poly(benzoxazine) have been used to produce coral-like porous carbons. The pyrolysis of the polymer followed by the removal of the silica produces a carbon with a continuous skeleton that contains spherical medium-size pores as "reservoirs" with a structure similar to a bunch of grapes. The total volume and the diameter of the "reservoir" pores are tunable. The coral-like morphology and the pore structure of the carbons make them suitable for use as electrode materials for supercapacitors and lithium-ion batteries. As supercapacitor electrodes, they exhibit excellent long-term cycle stability (almost no capacitance fading after 20 000 cycles at a current density of 1 A g^{-1}) and good rate capability with capacitance retention of 88% (from 0.1 A g^{-1} to 5 A g^{-1}). Meanwhile, as a matrix for the encapsulation of SnO_2 nanoparticles for Li-ion storage, the electrodes also show a high specific capacity and good cycling stability, i.e., 900 mA h g^{-1} after 50 charge−discharge cycles. The good electrochemical performance of such carbons shows that they are promising candidate electrode materials for electrochemical energy storage.

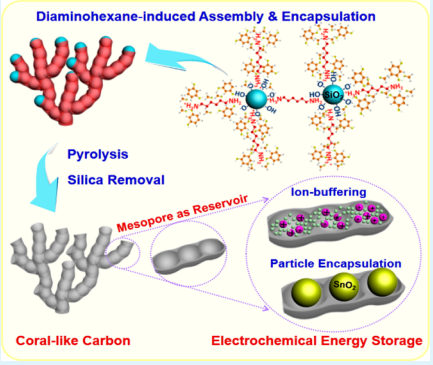

KEYWORDS: *diaminohexane, poly(benzoxazine), assembly, encapsulation, silica colloid, coral-like, porous carbon*

INTRODUCTION

Porous carbons used for energy storage have attracted widespread interest, because of their high surface area, good chemical stability, and electrical conductivity.[1−3] Porous carbons used as electrodes in supercapacitors are known to suffer from electrode kinetic problems due to in-pore ion-transport resistance and the diffusion distance. An inferior pore structure may lead to a significant electrode-potential drop and a surface area with low ion accessibility at large current density, severely reducing the performance of the electrode.[4−7] For a Li-ion battery, carbon materials are indispensible for providing a conductive phase to improve electron transport and buffer volume changes of the electrode materials (e.g., metal oxides) with low conductivity and poor stability.[1,8−11] Carbon coatings on the surface of these active materials are commonly used to increase the electrode conductivity and maintain the structure integrity of active materials during Li^+ insertion/extraction processes, leading to an improved cycle life of the batteries.[12] However, the carbon coating tightly adheres to the surface of the active materials, thus increasing the diffusion limitation for Li ions to reach their internal active core.[13] Therefore, porous carbons with embedded cavity and pore openings are favorable for use in electrochemical energy storage, as they can facilitate ion transport by providing easier diffusion pathways.[14−17]

Because size-/surface-dependent (e.g., structural, electrical, and mechanical) properties determine the energy storage performance,[18] great effort has been made to synthesize porous carbons with controlled morphologies and tunable pore structures.[19−24] For example, many different inorganic templates[25] (metal oxides, silica, zeolites) and supramolecular templates[26] (block co-polymers, surfactants, neutral amines) have been used to fabricate porous carbons with different pore types (cylindrical,[27,28] spherical,[29] worm-like[30]) and morphologies, such as spheres,[31−33] monoliths,[34−36] rods,[37] fibers,[38,39] membranes,[40] etc.[41−43] Mesoporous materials with identical mesopore surface areas have the largest pore volume when the mesopores are spherical, rather than other shapes. Such mesopores may serve as ion-buffering reservoirs to minimize the diffusion distance to the interior surfaces in supercapacitors, and also accommodate large volume changes of embedded active materials upon Li^+ insertion/extraction in Li-ion batteries. Colloidal silica has been demonstrated as a useful template for the preparation of porous carbon with spherical pores.[44−46] The conventional method involves the use of dried colloidal silica powder as the template, into which carbon precursors are infiltrated so that they fill the voids between particles in the silica aggregations.[47,48] The strict replication of

Received: January 24, 2014
Accepted: July 2, 2014
Published: July 2, 2014

   dx.doi.org/10.1021/am5034796 | ACS Appl. Mater. Interfaces 2014, 6, 11101−11109

morphology greatly depends on the mechanical strength and thermal stability of the carbon precursors.

Previously, we have developed a poly(benzoxazine-*co*-resol) system to produce porous carbon with designable pore structures and morphologies.[49,50] The polybenzoxazine-based carbon has a high mechanical strength and low thermal shrinkage. If the colloidal silica template can be dispersed into the polybenzoxazine system without phase separation, porous carbons with a continuous skeleton, good stability and abundant spherical pores, may eventually be prepared, which could be very useful in electrochemistry energy storage applications. It is envisaged that such porous carbons could be used not only as electrode materials for supercapacitors but also as effective matrices for the fabrication of hybrid anodes or cathodes for Li-ion batteries.

Recently, we have used one coral-like porous carbon, which was prepared through a polymerization of resorcinol with formaldehyde in the presence of diaminohexane and silica colloid and followed by a pyrolysis, to immobilize $LiFePO_4$ for better conductivity and diffusivity.[51] In this report, we present the formation mechanism of such coral-like structure and possibility of structure regulation. The detailed characterization results confirmed that 1,6-diaminohexane took crucial roles in determining the morphology. The 1,6-diaminohexane molecules anchor on the surfaces of the silica nanospheres, linking adjacent nanospheres and initiating the polymerization of benzoxazine on their surfaces in aqueous solution, which have not been reported before. The coral-like morphology and pore texture allow them potential applications for energy storage, so that their electrochemical performances are tested.

EXPERIMENTAL SECTION

Chemicals. Resorcinol (R, 99.5%) was purchased from Tianjin Kermel Chemical Reagent Co., Ltd. Formaldehyde solution (37 wt % formalin, F), 1,6-diaminohexane (DAH AR), $SnCl_4{\cdot}5H_2O$ (AR) and ammonia (AR) were supplied by Sinopharm Chemical Reagent Co., Ltd. Silica colloids (Ludox AS-40 40 wt %, Ludox HS-40 40 wt % and Ludox SM-30 30 wt %) were purchased from Sigma–Aldrich. All chemicals were used as received.

Synthesis of Carbon Materials. The carbon materials were prepared using colloidal silica as hard templates. Commercially available aqueous suspensions of silica colloids Ludox AS-40, Ludox HS-40, and Ludox SM-30 (with an average colloid particle diameter of 22, 12, and 7 nm, respectively) were used directly in the synthesis.

Typically, 2 mmol resorcinol was first dissolved in deionized water (100 g) with vigorous stirring at room temperature and then 4 mmol formaldehyde (37 wt %) was added to form a clear solution. Subsequently, a certain amount of Ludox was added to the clear solution followed by 0.5 mmol DAH. The resultant solution was then heated to 80 °C accompanied by vigorous stirring for 42 h. The obtained silica/polymer compounds were pyrolyzed at 800 °C for 2 h under nitrogen atmosphere. Mesoporous carbon was obtained after the removal of the silica template using an aqueous NaOH solution.

The molar ratios of SiO_2 to resorcinol (denoted SiO_2:R) were 2:1, 3.5:1, 5:1, 8:1, and 12:1, and the carbon materials obtained were respectively denoted PBC-*x*-1, PBC-*x*-2, PBC-*x*-3, PBC-*x*-4 and PBC-*x*-5 (where *x* represents different templates, e.g., PBC-HS corresponds to Ludox HS-40 as templates).

Synthesis of SnO_2/Carbon Materials. The SnO_2@carbon (SnO_2@C) materials were prepared using in situ ammonia treatment and subsequent pyrolysis. First, 2 M of $SnCl_4{\cdot}5H_2O$ in ethanol was mixed with the carbon matrix using wet-impregnation. Subsequently, the mixture was treated in an ammonia atmosphere in order to covert the $SnCl_4{\cdot}5H_2O$ into an $Sn(OH)_4$ intermediate, followed by washing and drying. The impregnation, conversion, washing and drying steps were repeated until the desired amount of SnO_2 loading was reached. Finally, the sample was heated at 550 °C for 3 h under an argon atmosphere to obtain the final SnO_2@C material.

Characterization. Scanning electron microscopy (SEM) investigations were carried out with a FEI Nova NanoSEM 450 instrument. Transmission electron microscopy (TEM) analyses were carried out with FEI Tecnai $G^2$20S-Twin equipment operating at 200 kV. N_2 adsorption isotherms were measured with a Micromeritics Tristar 3000 adsorption analyzer. Prior to each adsorption experiment, the sample was degassed for 6 h at 200 °C, ensuring that the residual pressure fell below 5×10^{-3} mbar, and then cooled to the target temperature, followed by the introduction of a single-component gas (N_2) into the system. The Brunauer–Emmett–Teller (BET) method was used to calculate the specific surface area. The pore size distribution was derived from the adsorption branches of the isotherms using the Barrett–Joyner–Halenda (BJH) model. Total pore volumes were calculated from the amount adsorbed at a relative pressure (P/P_0) of 0.95. The micropore volume was calculated by the *t*-plot analysis. Zeta potentials of the samples were measured using Malvern Zetasizer Nano ZS90.

Electrochemical Measurements. The capacitive performance of all carbon samples was investigated in 6 M KOH using two-electrode cells. The working electrode was prepared by mixing active materials, polytetrafluoroethylene (PTFE), and conductive additive (Super P) (80:10:10 by weight) in 7 mL of ethanol followed by ultrasonication. The slurry of the mixture was put onto a foam nickel current collector and pressed under a pressure of 10 MPa for 5 min to fabricate an electrode. Two electrodes with identical mass were selected to prepare a sandwich-type cell using a membrane filter (MPF50AC, Nippon Kodoshi Corporation, Japan) as a separator. The capacitive performance of the cells was estimated using a Model CHI660D electrochemical workstation (CH Instruments, Inc., Shanghai, China) at 25 °C. Cyclic voltammetry (CV), galvanostatic charge/discharge cycling (GC) and electrochemical impedance spectroscopy (EIS) were used to evaluate the electrochemical performance of the electrodes. Stability measurements were carried out using a multichannel electrochemical workstation (Arbin Instruments USA). The specific capacitance of one electrode (C) was calculated from the discharge process after 20 cycles of activation, according to the formula below:

$$C = 4 \times \frac{I\Delta t}{\Delta V}$$

where I is the discharge current density based on the total mass of active material in the two electrodes (A g^{-1}), Δt is the discharge time (in seconds), and ΔV is the potential window from the end of the internal resistance (R) drop to the end of the discharge process. (in volts)

Li-ion battery electrochemical measurements were carried out using CR2025 coin-type cells with lithium metal as the counter and reference electrodes. The electrolyte was 1 M $LiPF_6$ dissolved in a mixture of dimethyl carbonate (DMC), diethyl carbonate (DEC), and ethylene carbonate (EC) (1:1:1 by volume). The working electrode consisted of 80 wt % of the active material, 10 wt % of conductive carbon black, and 10 wt % of binder (polyvinylidene difluoride, PVDF). A typical electrode disk (~12 mm in diameter) weighed ~3 mg based on the total mass of SnO_2 and carbon. Galvanostatic charge/discharge tests were performed on a LAND CT2001A battery tester.

RESULTS AND DISCUSSION

The size and morphology of the carbon samples were characterized by scanning electron microscopy (SEM). As shown in Figure 1, the carbon matrix possesses a coral-like morphology with a branch-like continuous skeleton and a spherical open mesopore at the surface. Sample PBC-AS-1 (SiO_2:R = 2:1) using 22 nm silica nanospheres has a carbon wall of 13 nm with an open pore of ~18 nm (Figure 1a). The porosity of the materials was adjustable using different amounts of the Ludox precursor. When increasing the molar ratio of SiO_2:R, the obtained carbons show larger pore volumes and a

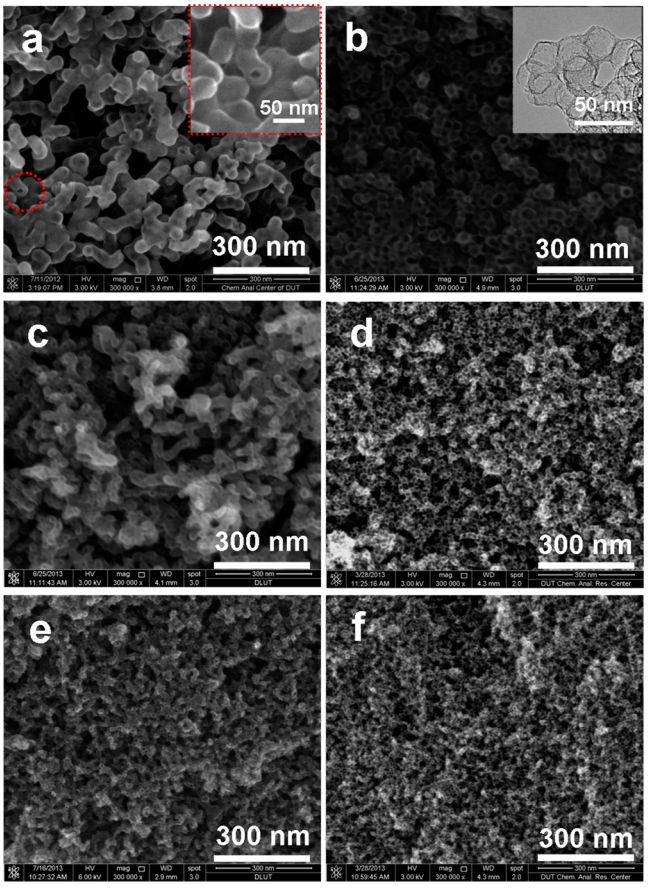

Figure 1. SEM images of (a) PBC-AS-1, (b) PBC-AS-3, and (c) PBC-HS-1, (d) PBC-HS-3, (e) PBC-SM-1 and (f) PBC-SM-3. The inset of panel a is a magnified image, and the inset of panel b is a TEM image.

lower carbon wall thickness. After increasing the molar ratio to SiO_2:R = 5:1, PBC-AS-3 shows a thinner carbon wall of 6 nm with a larger open pore of ~22 nm. A transmission electron microscopy (TEM) image of PBC-AS-3 (Figure 1b) shows that the carbon matrix is composed of vesicles that have a cavity diameter of ~22 nm, similar to that of the silica nanoparticle template. This open pore structure is conducive to the transmission of mobile species. The mesopores could also serve as ion-buffering reservoirs to minimize the diffusion distance to the interior surfaces.

An analogous sample synthesized in the absence of DAH shows an irregular carbon structure (see Figure S1 in the Supporting Information). Therefore, we deduce that the use of DAH in the synthesis facilitates the formation of the coral-like structure. The skeleton width of the coral-like carbon materials changes when using different sizes of silica nanospheres as the template. Sample PBC-HS-1 (Figure 1c) using silica nanospheres ~12 nm in diameter shows a skeleton width of ~25 nm. For silica nanospheres ~7 nm in diameter, the carbon (PBC-SM-1, Figure 1e) shows the smallest skeleton width of ~17 nm. Therefore, the DAH molecules are speculated to attach to the surfaces of the silica nanospheres and induce colloid assembly and poly(benzoxazine) surface coating.

In order to clarify whether diaminohexane molecules are attached to the silica nanospheres, the zeta potentials of a colloidal silica solution mixed with different amounts of DAH were measured. It is known that the isoelectric point of silica is at a pH of ~2.[52] The commercial Ludox colloidal silica nanospheres are actually stabilized in alkaline solutions (pH 9.1−9.5). Under this condition, the surfaces of the silica display mostly $-O^-$ groups, usually surrounded by NH_4^+ or Na^+ through electrostatic interaction (which stabilizes the silanols and prevents cross-linking) being responsible for colloidal stability.

The negatively charged original Ludox-HS (Figure 2a) indicates the predominance of $-O^-$ groups on the silica surface, and its zeta potential value is approximately −36 mV. After adding a certain concentration of DAH, the zeta potential decreases by degrees. A plateau of ca. 1 mV was reached at ~150 mM and no evident potential change occurs with a further increase in DAH concentration. The changes and the small reversal of zeta potential indicate that diamine molecules are attached to the surface of the silica nanospheres.

When an alkali solution with a pH value (DAH 9.2, NaOH 9.3, ammonia 9.4) was added to the colloidal silica, only the one with added DAH precipitated rapidly, which may be due to the two $-NH_2$ groups of a DAH molecule connecting adjacent silica nanospheres, while the others remain colloidal, as shown in Figure 2b.

Generally, there are two driving forces for the adsorption of molecules onto the surface of oxide particles in an aqueous solution, one is the electrostatic attraction between the particle surfaces and ionized molecules, and the other is the specific chemical reaction or hydrogen-bonding interaction between the functional groups of adsorbate molecules and the surface of oxide particles.[53,54] In the case of DAH molecules, the

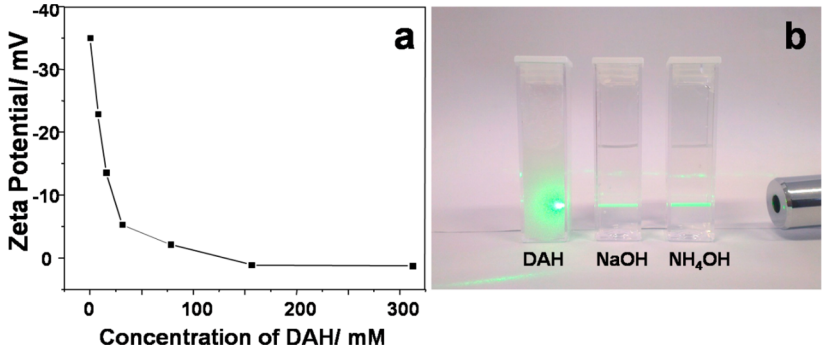

Figure 2. (a) Zeta potential of Ludox-HS-40 modified with diaminohexane in aqueous dispersions after 48 h. The particle concentration in the dispersions is 17 wt %. (b) An optical photograph of colloidal silica (Ludox-HS-40) added to three different alkali solutions with similar pH (diaminohexane 9.2, NaOH 9.3, ammonia 9.4).

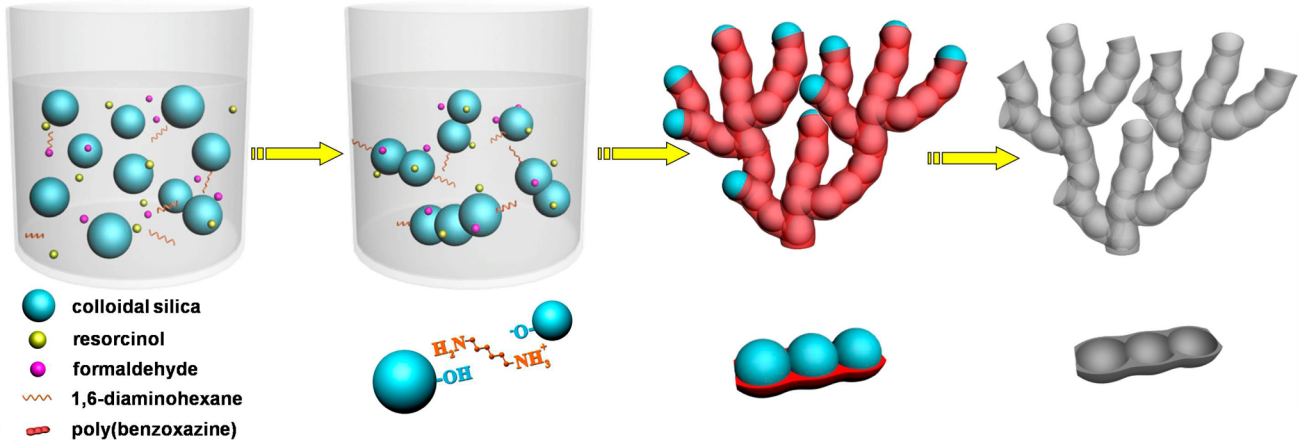

Figure 3. Diagram for the formation process of the coral-like carbon.

protonation of the amine group occurs when the pH value in an aqueous solution is close to or lower than the pK_a value of the functional group $-NH_2$. The pK_{a1} and pK_{a2} values of DAH are 9.83 and 10.93, respectively.[55] In the current synthesis, the pH values are between 9.3 and 11.3 and the amine groups can be protonated in aqueous solutions, so that they would then attach to the negatively charged particle surface by electrostatic interaction (Figure 2a). The protonation degree varies as the pH of the aqueous medium changes.[55] DAH molecules with a higher degree of protonation would more easily attach to the surface of the silica particles. In addition to the electrostatic attraction, the adsorption may also include weak hydrogen-bonding interactions between the amine groups and the silanol groups on the silica surfaces.[56,57] Thus, the diamine (DAH) molecules are considered the key to link adjacent silica nanospheres. Meanwhile, the DAH induces the benzoxazine precursor to polymerize on the surface of the silica nanospheres resulting in the observed coral-like carbon materials. The proposed mechanism is summarized in Figure 3.

Nitrogen adsorption measurements were performed to determine the pore structure of the prepared carbons (see Figure 4, as well as Figures S2 and S3 in the Supporting Information). Taking PBC-HS as an example, all the isotherms feature hysteresis between the desorption and adsorption branches (Figure 4a), indicating the presence of mesopores. The hysteresis loops in the nitrogen adsorption isotherms (PBC-HS-2 and PBC-HS-3 at P/P_0 = 0.6−0.95, PBC-HS-1 at P/P_0 = 0.5−0.9) of carbon materials obtained with SiO_2:R ≤ 5 present the characteristic of a type H1 loop, which may certify the good mesopore connectivity and good degree of pore-size uniformity. When SiO_2:R > 5, the hysteresis loop turns to type H2 (PBC-HS-5), indicating the mesopore connectivity turned bad. The pore size distribution curve of PBC-HS (Figure 4b) shows that the coral-like carbon obtained with SiO_2:R ≤ 5 has a bimodal pore size distribution at ca. 2 nm and 12−14 nm. These are respectively attributed to small pores in the carbon skeleton wall and the interior mesopores of the coral-like carbon. The defined mesopore size is very close to the average size of the silica nanoparticles, and the measured SiO_2 content of the obtained polymer−silica composite is close to their theoretical content (see Figure S4 in the Supporting Information), which confirms the templating effect of the silica nanoparticles, the DAH-triggered surface coating of the silica particles, and the good thermal stability of polybenzoxazine during carbonization.

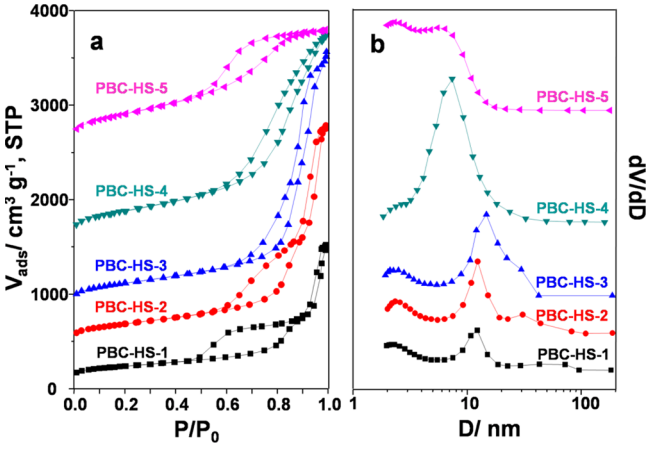

Figure 4. (a) Nitrogen adsorption isotherms and (b) the corresponding BJH pore size distribution of the coral-like carbon (PBC-HS) templated from Ludox-HS-40 with different mass %. The isotherms of PBC-HS-2, PBC-HS-3, PBC-HS-4, and PBC-HS-5 at standard temperature and pressure (STP) were offset vertically by 400, 800, 1500, and 2500 cm^3 g^{-1}, respectively.

The pore structure parameters of each sample are listed in Table 1 and Table S1 in the Supporting Information. With an increase in SiO_2:R ratio, the total pore volume and BET surface area of the carbon increase gradually. As the SiO_2:R ratio increases to a specific value, the pore volume decreases and the pore size becomes smaller, which is attributed to pore collapse. PBC-SM-3 has the largest total volume, up to 4.18 cm^3 g^{-1}. Such a big volume would, to a great extent, allow the storage of the active materials of a Li-ion battery or the electrolyte of supercapacitors. By fitting the experimental data of SiO_2:R and the total pore volume of the carbon, a good linear relationship between the pore volume and SiO_2:R ratio was obtained (Figure 5). Hence, our synthesis method is demonstrated to produce coral-like carbons with a controlled pore volume and pore size distribution by appropriately changing the SiO_2:R ratio. These results also provide a strong indication that the carbon precursor has successfully coated the silica surfaces due to the interaction between the silica particles and DAH molecules. The tap density of the prepared carbons is small, and no obvious relations between tap density and the ratio of SiO_2:R in the view of PBC-HS series. However, the carbon with

Table 1. Structural Properties of the Carbons Prepared Using Different Templates and SiO_2:R Ratios

sample	$n_{SiO_2}:n_R$ (mol:mol)	S_{BET} (m^2 g^{-1})	V_{total} [a] (cm^3 g^{-1})	V_{micro} [b] (cm^3 g^{-1})	D_{pore} [c] (nm)
PBC-AS-1	2:1	563	0.85	0.12	2, 24
PBC-AS-2	3.5:1	878	1.68	0.14	2, 22
PBC-AS-3	5:1	977	2.33	0.10	2, 22
PBC-AS-4	8:1	1086	3.26	0.08	2, 23
PBC-AS-5	12:1	1197	2.62	0.08	2, 17
PBC-HS-1	2:1	831	1.35	0.13	2, 12
PBC-HS-2	3.5:1	988	2.52	0.12	2, 12
PBC-HS-3	5:1	1120	3.70	0.12	2, 14
PBC-HS-4	8:1	1326	3.17	0.06	2, 7
PBC-HS-5	12:1	1462	1.96	0.03	2, 6
PBC-SM-1	2:1	963	1.85	0.09	2, 8
PBC-SM-2	3.5:1	1264	3.09	0.13	2, 8
PBC-SM-3	5:1	1374	4.18	0.02	2, 7, 18

[a] V_{total}: total pore volume at P/P_0 = 0.95. [b] V_{micro}: micropore volume calculated by the *t*-plot analysis. [c] Pore diameter at the maximum of the pore size distribution calculated from the adsorption branch via the BJH method.

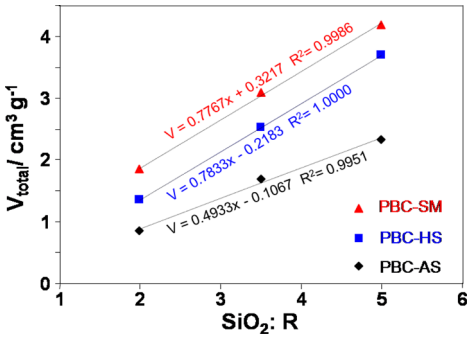

Figure 5. Relationship between the molar ratio of SiO_2 to resorcinol and the total pore volume of the coral-like carbons.

bigger pore size present smaller tap density (see Table S1 in the Supporting Information).

Because the large pore volume allows ion-buffering and a high surface area for ion storage and the continuous carbon skeleton allows good electrical conductivity, these carbon materials have been investigated as electrode materials for supercapacitors. The measured CV curves for PBC-AS-3, PBC-HS-3, and PBC-SM-3 in two-electrode cells at 10 mV s^{-1} present rectangular shapes (Figure 6a), indicating an ideal capacitive behavior and a fast charge/discharge characteristic. All the electrodes show nearly linear charge/discharge curves (Figure 6b) at a current density of 0.5 A g^{-1}, which indicates ideal double layer capacitive behavior. The micropore is considered to be beneficial space to store charge for carbon-based supercapacitors.[58] The small micropore volume of the prepared carbon (Table 1) makes them present low specific capacity. However, note that the capacitance retention ratios of the samples are as high as 85%−88%, even when the current density is increased from 0.1 A g^{-1} to 5 A g^{-1} (Figure 6c). The good rate capability implies a high electrical conductivity of such a coral-like skeleton and a small ion-transport distance due to the ion-buffering "reservoir".

Figure 7a shows the Nyquist plots of the cells. The impedance data is plotted as the real component of impedance, Z_{real}, with equivalent series resistance subtracted which is the intersection of the plots at the *X*-axis. In all cases, a straight line is obtained in the low-frequency range. The imaginary part of the impedance spectra at low frequencies represents the capacitive behavior of the electrode and approaches a vertical line for an ideal capacitor.[59] Almost no semicircle is observed in the high-frequency region, indicating fast charge transfer in the open mesopores. The length of the line with a slope of ~45°, caused by diffusion impedance and being known as the Warburg impedance, increases from PBC-AS-3 to PBC-SM-3. PBC-AS-3 showed the lowest Warburg impedance, because it provided the easiest ion diffusion within the mesopores of the electrodes. The capacitance increases with decreasing frequency (100 kHz to 10 mHz) in an inverse S-shaped mode (Figure 7b). These results prove that the supercapacitors have a long platform in the low-frequency range, because of fast ion transport and rapid ion adsorption and desorption on the surface. Moreover, the capacitance increases in the order of PBC-SM-3 < PBC-HS-3 < PBC-AS-3 for frequencies >10 Hz, which further confirms the importance of creating easy ion-transport pathways in attempts to produce high-rate supercapacitor electrodes.

The long-term cycle stability at a current density of 1 A g^{-1} is presented in Figure 6d. The capacitance increases during the first 5000 cycles, which is attributed an activation process of the material. After 20 000 cycles, a very small decrease in the initial special capacitance is observed. The capacitance retention of the samples is close to 100%, indicating a high stability of the skeleton structure and no pore collapse after such long-term cycles.

Our previous studies have demonstrated that mesoporous carbon could improve the conductivity/diffusivity of the encapsulated $LiFePO_4$ to achieve high-performance Li-ion storage.[51] The SnO_2 has a high theoretical capacity of 1494 mA h g^{-1}, but suffers from severe capacity fading, because of the large volume change of ~250% and serious aggregation of Sn clusters during cycling.[60] Following this idea, we have used these coral-like carbons as matrices to buffer the volume expansion of SnO_2 nanoparticles, because of the high mechanical strength of the polybenzoxazine-based carbon, and we have studied their performance for Li-ion batteries. From the TG curves shown in Figure S5 in the Supporting Information, it is observed that the loadings of SnO_2 in the carbons are similar and can approach 80 wt %. The SnO_2 nanoparticles are encapsulated in the mesopores and there is no visible agglomeration (see Figure S6 in the Supporting Information).

The cycling performance of these anodes was examined at a current density of 200 mA g^{-1} over a voltage range of 0.005−3 V (Figure 8a). Sample SnO_2@PBC-SM-3 shows the highest Li^+ storage capacity and the most-stable cycle performance, compared with the other two samples. After 50 cycles, the reversible capacity of SnO_2@PBC-SM-3 remains ~900 mAh g^{-1} (based on the total mass of SnO_2 and carbon) and the corresponding capacity retention measured after the second

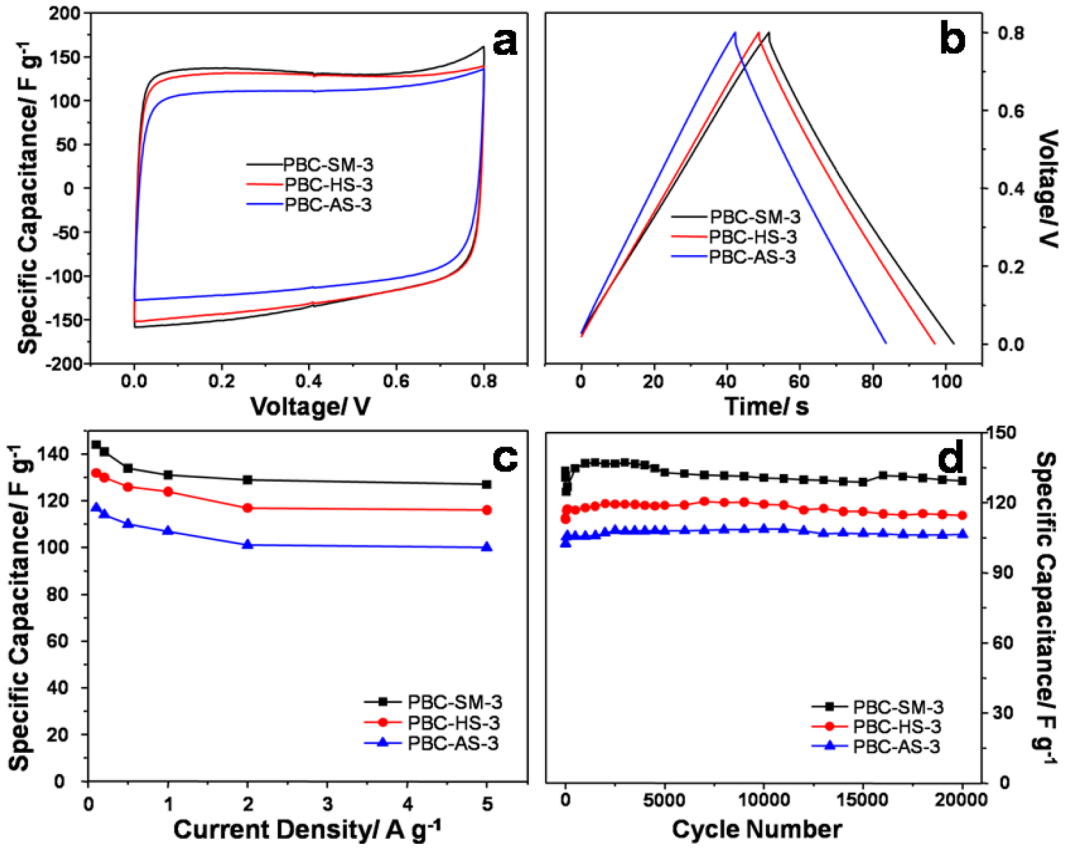

Figure 6. (a) Cyclic voltammograms at 10 mV s^{-1}, (b) galvanostatic charge/discharge curves at 0.5 A g^{-1}, (c) specific capacitances at different current densities, and (d) long-term cycling of the carbon samples.

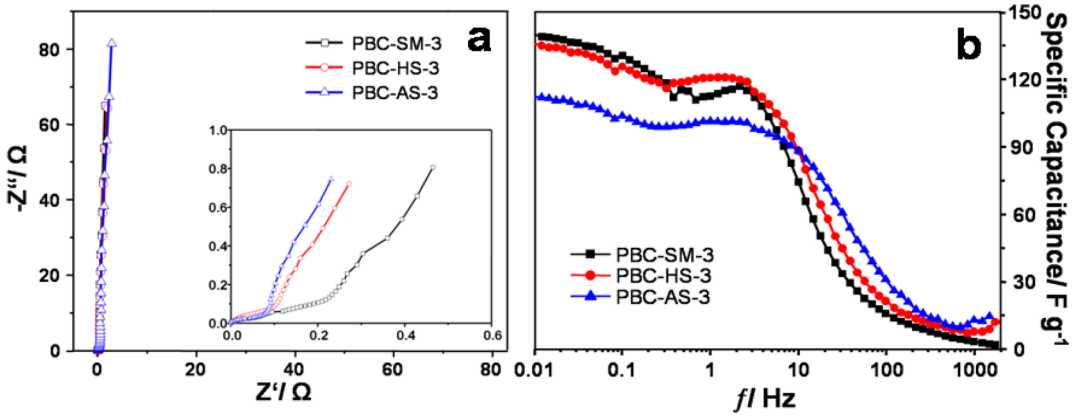

Figure 7. (a) Nyquist plots measured between 100 kHz and 10 mHz and (b) specific capacitance of the carbon samples versus frequency.

cycle is 94%. Both the capacity and cycle performance are better than that of recently reported SnO_2 nanoparticles compounded with three-dimensional (3D) macroporous carbon[61] and graphene.[62,63] In Figure 8b, the Nyquist plots of all SnO_2@C samples exhibit a broad depressed semicircle in the medium frequency range, which shows that the charge transfer resistance results from charge-transfer kinetics.[64,65] The size of the semicircle increases gradually from SnO_2@PBC-SM-3 to SnO_2@PBC-AS-3, indicating a substantial increase of charge-transfer resistance with increasing pore size of the carbon matrix. One thus can deduce that the electrochemical performance of the SnO_2@C samples strongly depends on the size of the SnO_2 nanoparticles, which is affected by the pore size of the pristine carbon matrix. Smaller and open pores warrant the formation of smaller SnO_2 crystals, thus allowing more efficient physical contact between the active material and the carbon matrix during cycling.

CONCLUSIONS

A coral-like carbon structure was prepared by a 1,6-diaminohexane-induced silica colloid assembly and a poly(benzoxazine) surface coating method. The carbon materials show a continuous skeleton with embedded bunch of small and open mesopores. It should be emphasized that the volume and diameter of the mesoporous reservoir are controllable. Their coral-like morphology and spherical pore structure make the carbons good electrode materials for supercapacitors and Li-ion batteries. When used as supercapacitor electrodes, they exhibit

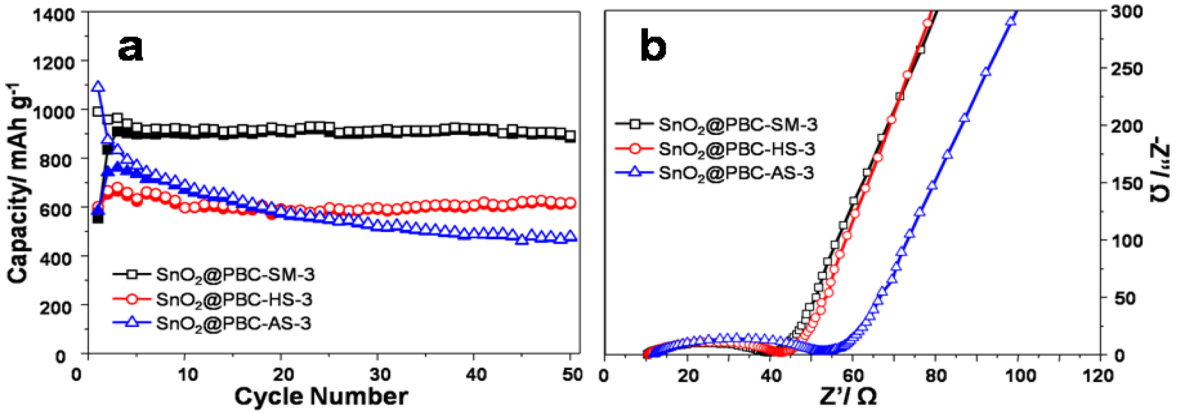

Figure 8. (a) Cycling performances of SnO_2@PBC-SM-3, SnO_2@PBC-HS-3, and SnO_2@PBC-AS-3 at a current density of 200 mA g^{-1} over a voltage range of 0.005−3 V; (b) the Nyquist plots.

excellent long-term cycle stability, almost no capacitance fading after 20 000 cycles at a current density of 1 A g^{-1}, and good rate capability with capacitance retention of 88% in the current range of 0.1−5 A g^{-1}. When the carbon was used as a matrix for the encapsulation of SnO_2 nanoparticles for lithium storage, the batteries showed a high specific capacity and good cycling stability. The excellent electrochemical performance of such coral-like carbons is attributed to their properties, such as large pore volume, high surface area, and unique continuous carbon skeleton. This makes them an alternative promising electrode material for electrochemical energy storage.

■ ASSOCIATED CONTENT

Supporting Information

SEM image of a carbon prepared using the same procedure of PBC-AS-1, but without DAH; nitrogen adsorption isotherms and the corresponding BJH pore size distribution of the coral-like carbon (PBC-AS and PBC-SM); table of the tap density of the coral-like carbon; TG curves of SnO_2@PBC-SM-3, SnO_2@PBC-HS-3 and SnO_2@PBC-AS-3; SEM image of Sn@PBC-AS-3. This material is available free of charge via the Internet at http://pubs.acs.org.

■ AUTHOR INFORMATION

Corresponding Author

*Tel./Fax: +86-0411-84986112. E-mail: anhuilu@dlut.edu.cn.

Notes

The authors declare no competing financial interest.

■ ACKNOWLEDGMENTS

The project was supported by the Special Program for Basic Research of the Ministry of Science and Technology (No. 2012CB626802) and National Program on Key Basic Research Project (973 Program, No. 2013CB934104).

■ REFERENCES

(1) Zhai, Y.; Dou, Y.; Zhao, D.; Fulvio, P. F.; Mayes, R. T.; Dai, S. Carbon Materials for Chemical Capacitive Energy Storage. *Adv. Mater.* **2011**, *23*, 4828−4850.

(2) Wang, D.; Zeng, Q.; Zhou, G.; Yin, L.; Li, F.; Cheng, H. M.; Gentle, I. R.; Lu, G. Q. Carbon/Sulfur Composites for Li-S Batteries: Status and Prospects. *J. Mater. Chem. A* **2013**, *1*, 9382−9394.

(3) Wang, G.; Zhang, L.; Zhang, J. A Review of Electrode Materials for Electrochemical Supercapacitors. *Chem. Soc. Rev.* **2012**, *41*, 797−828.

(4) Wang, D. W.; Li, F.; Liu, M.; Lu, G. Q.; Cheng, H. M. 3D Aperiodic Hierarchical Porous Graphitic Carbon Material for High-Rate Electrochemical Capacitive Energy Storage. *Angew. Chem., Int. Ed.* **2007**, *47*, 373−376.

(5) Wang, D. W.; Li, F.; Fang, H. T.; Liu, M.; Lu, G. Q.; Cheng, H. M. Effect of Pore Packing Defects in 2-D Ordered Mesoporous Carbons on Ionic Transport. *J. Phys. Chem. B* **2006**, *110*, 8570−8575.

(6) Song, H. K.; Hwang, H. Y.; Lee, K. H.; Dao, L. H. The Effect of Pore Size Distribution on the Frequency Dispersion of Porous Electrodes. *Electrochim. Acta* **2000**, *45*, 2241−2257.

(7) Long, J. W.; Dunn, B.; Rolison, D. R.; White, H. S. Three-Dimensional Battery Architectures. *Chem. Rev.* **2004**, *104*, 4463−4492.

(8) Wu, Z. S.; Ren, W.; Wen, L.; Gao, L.; Zhao, J.; Chen, Z.; Zhou, G.; Li, F.; Cheng, H. M. Graphene Anchored with Co_3O_4 Nanoparticles as Anode of Lithium Ion Batteries with Enhanced Reversible Capacity and Cyclic Performance. *ACS Nano* **2010**, *4*, 3187−3194.

(9) Yang, S.; Yue, W.; Zhu, J.; Ren, Y.; Yang, X. Graphene-based Mesoporous SnO_2 with Enhanced Electrochemical Performance for Lithium-Ion Batteries. *Adv. Funct. Mater.* **2013**, *23*, 3570−3576.

(10) Scrosati, B. Recent Advances in Lithium Ion Battery Materials. *Electrochim. Acta* **2000**, *45*, 2461−2466.

(11) Wang, D.; Kou, R.; Choi, D.; Yang, Z.; Nie, Z.; Li, J.; Saraf, L. V.; Hu, D.; Zhang, J.; Graff, G. L.; et al. Ternary Self-assembly of Ordered Metal Oxide-Graphene Nanocomposites for Electrochemical Energy Storage. *ACS Nano* **2010**, *4*, 1587−1595.

(12) Li, H.; Zhou, H. Enhancing the Performances of Li-Ion Batteries by Carbon-Coating: Present and Future. *Chem. Commun.* **2012**, *48*, 1201−1217.

(13) Zhou, G.; Wang, D. W.; Li, F.; Zhang, L.; Li, N.; Wu, Z. S.; Wen, L.; Lu, G. Q.; Cheng, H. M. Graphene-Wrapped Fe_3O_4 Anode Material with Improved Reversible Capacity and Cyclic Stability for Lithium Ion Batteries. *Chem. Mater.* **2010**, *22*, 5306−5313.

(14) Lou, X. W.; Deng, D.; Lee, J. Y.; Archer, L. A. Preparation of SnO_2/Carbon Composite Hollow Spheres and Their Lithium Storage Properties. *Chem. Mater.* **2008**, *20*, 6562−6566.

(15) Zhang, W.; Huang, Z. H.; Zhou, C.; Cao, G.; Kang, F.; Yang, Y. Porous Carbon for Electrochemical Capacitors Prepared from a Resorcinol/Formaldehyde-based Organic Aquagel with Nano-Sized Particles. *J. Mater. Chem.* **2012**, *22*, 7158−7163.

(16) Zhang, W.; Huang, Z. H.; Cao, G.; Kang, F.; Yang, Y. A Novel Mesoporous Carbon with Straight Tunnel-like Pore Structure for High Rate Electrochemical Capacitors. *J. Power Sources* **2012**, *204*, 230−235.

(17) Wang, G.; Liu, H.; Liu, J.; Qiao, S.; Lu, G. M.; Munroe, P.; Ahn, H. Mesoporous $LiFePO_4$/C Nanocomposite Cathode Materials for High Power Lithium Ion Batteries with Superior Performance. *Adv. Mater.* **2010**, *22*, 4944−4948.

(18) Dai, L.; Chang, D. W.; Baek, J. B.; Lu, W. Carbon Nanomaterials for Advanced Energy Conversion and Storage. *Small* **2012**, *8*, 1130−1166.

(19) Ryoo, R.; Joo, S. H.; Kruk, M.; Jaroniec, M. Ordered Mesoporous Carbons. *Adv. Mater.* **2001**, *13*, 677−681.
(20) Stein, A.; Wang, Z.; Fierke, M. A. Functionalization of Porous Carbon Materials with Designed Pore Architecture. *Adv. Mater.* **2009**, *21*, 265−293.
(21) Lee, J.; Kim, J.; Hyeon, T. Recent Progress in the Synthesis of Porous Carbon Materials. *Adv. Mater.* **2006**, *18*, 2073−2094.
(22) Wan, Y.; Shi, Y.; Zhao, D. Supramolecular Aggregates as Templates: Ordered Mesoporous Polymers and Carbons. *Chem. Mater.* **2007**, *20*, 932−945.
(23) Liang, C.; Li, Z.; Dai, S. Mesoporous Carbon Materials: Synthesis and modification. *Angew. Chem., Int. Ed.* **2008**, *47*, 3696−3717.
(24) Ma, T. Y.; Liu, L.; Yuan, Z. Y. Direct Synthesis of Ordered Mesoporous Carbons. *Chem. Soc. Rev.* **2013**, *42*, 3977−4003.
(25) Lee, J.; Han, S.; Hyeon, T. Synthesis of New Nanoporous Carbon Materials Using Nanostructured Silica Materials as Templates. *J. Mater. Chem.* **2004**, *14*, 478−486.
(26) Feng, D.; Lv, Y.; Wu, Z.; Dou, Y.; Han, L.; Sun, Z.; Xia, Y.; Zheng, G.; Zhao, D. Free-Standing Mesoporous Carbon Thin Films with Highly Ordered Pore Architectures for Nanodevices. *J. Am. Chem. Soc.* **2011**, *133*, 15148−15156.
(27) Joo, S. H.; Choi, S. J.; Oh, I.; Kwak, J.; Liu, Z.; Terasaki, O.; Ryoo, R. Ordered Nanoporous Arrays of Carbon Supporting High Dispersions of Platinum Nanoparticles. *Nature* **2001**, *412*, 169−172.
(28) Wang, X.; Liang, C.; Dai, S. Facile Synthesis of Ordered Mesoporous Carbons with High Thermal Stability by Self-Assembly of Resorcinol−Formaldehyde and Block Copolymers under Highly Acidic Conditions. *Langmuir* **2008**, *24*, 7500−7505.
(29) Han, S.; Hyeon, T. Novel Silica-Sol Mediated Synthesis of High Surface Area Porous Carbons. *Carbon* **1999**, *37*, 1645−1647.
(30) Lee, J.; Yoon, S.; Oh, S. M.; Shin, C. H.; Hyeon, T. Development of a New Mesoporous Carbon Using an HMS Aluminosilicate Template. *Adv. Mater.* **2000**, *12*, 359−362.
(31) Liu, R.; Mahurin, S. M.; Li, C.; Unocic, R. R.; Idrobo, J. C.; Gao, H.; Pennycook, S. J.; Dai, S. Dopamine as a Carbon Source: the Controlled Synthesis of Hollow Carbon Spheres and Yolk-Structured Carbon Nanocomposites. *Angew. Chem., Int. Ed.* **2011**, *50*, 6799−6802.
(32) Fuertes, A. B.; Valle-Vigón, P.; Sevilla, M. One-Step Synthesis of Silica@ Resorcinol-Formaldehyde Spheres and Their Application for the Fabrication of Polymer and Carbon Capsules. *Chem. Commun.* **2012**, *48*, 6124−6126.
(33) Yoon, S. B.; Sohn, K.; Kim, J. Y.; Shin, C. H.; Yu, J. S.; Hyeon, T. Fabrication of Carbon Capsules with Hollow Macroporous Core/Mesoporous Shell Structures. *Adv. Mater.* **2002**, *14*, 19−21.
(34) Yang, H.; Shi, Q.; Liu, X.; Xie, S.; Jiang, D.; Zhang, F.; Yu, C.; Tu, B.; Zhao, D. Synthesis of Ordered Mesoporous Carbon Monoliths with Bicontinuous Cubic Pore Structure of *Ia3d* Symmetry. *Chem. Commun.* **2002**, 2842−2843.
(35) Hao, G. P.; Li, W. C.; Wang, S.; Wang, G. H.; Qi, L.; Lu, A. H. Lysine-Assisted Rapid Synthesis of Crack-Free Hierarchical Carbon Monoliths with a Hexagonal Array of Mesopores. *Carbon* **2011**, *49*, 3762−3772.
(36) Fan, L. Z.; Hu, Y. S.; Maier, J.; Adelhelm, P.; Smarsly, B.; Antonietti, M. High Electroactivity of Polyaniline in Supercapacitors by Using a Hierarchically Porous Carbon Monolith as a Support. *Adv. Funct. Mater.* **2007**, *17*, 3083−3087.
(37) Yu, C.; Fan, J.; Tian, B.; Zhao, D.; Stucky, G. D. High-Yield Synthesis of Periodic Mesoporous Silica Rods and Their Replication to Mesoporous Carbon Rods. *Adv. Mater.* **2002**, *14*, 1742−1745.
(38) Chen, L. F.; Zhang, X. D.; Liang, H. W.; Kong, M.; Guan, Q. F.; Chen, P.; Wu, Z. Y.; Yu, S. H. Synthesis of Nitrogen-Doped Porous Carbon Nanofibers as an Efficient Electrode Material for Supercapacitors. *ACS Nano* **2012**, *6*, 7092−7102.
(39) Elazari, R.; Salitra, G.; Garsuch, A.; Panchenko, A.; Aurbach, D. Sulfur-Impregnated Activated Carbon Fiber Cloth as a Binder-Free Cathode for Rechargeable Li-S Batteries. *Adv. Mater.* **2011**, *23*, 5641−5644.
(40) Song, L.; Feng, D.; Campbell, C. G.; Gu, D.; Forster, A. M.; Yager, K. G.; Fredin, N.; Lee, H.; Jones, R. L.; Zhao, D. Y.; et al. Robust Conductive Mesoporous Carbon-Silica Composite Films with Highly Ordered and Oriented Orthorhombic Structures from Triblock−Copolymer Template Co-Assembly. *J. Mater. Chem.* **2010**, *20*, 1691−1701.
(41) Lee, J.; Sohn, K.; Hyeon, T. Fabrication of Novel Mesocellular Carbon Foams with Uniform Ultralarge Mesopores. *J. Am. Chem. Soc.* **2001**, *123*, 5146−5147.
(42) Kim, J.; Lee, J.; Hyeon, T. Direct Synthesis of Uniform Mesoporous Carbons from the Carbonization of As-Synthesized Silica/Triblock Copolymer Nanocomposites. *Carbon* **2004**, *42*, 2711−2719.
(43) Jun, S.; Joo, S. H.; Ryoo, R.; Kruk, M.; Jaroniec, M.; Liu, Z.; Ohsuna, T.; Terasaki, O. Synthesis of New, Nanoporous Carbon with Hexagonally Ordered Mesostructure. *J. Am. Chem. Soc.* **2000**, *122*, 10712−10713.
(44) Jaroniec, M.; Choma, J.; Gorka, J.; Zawislak, A. Colloidal Silica Templating Synthesis of Carbonaceous Monoliths Assuring Formation of Uniform Spherical Mesopores and Incorporation of Inorganic Nanoparticles. *Chem. Mater.* **2007**, *20*, 1069−1075.
(45) Li, X.; Cao, Y.; Qi, W.; Saraf, L. V.; Xiao, J.; Nie, Z.; Jaroniec, M.; Zhang, J. G.; Schwenzer, B.; Liu, J. Optimization of Mesoporous Carbon Structures for Lithium-Sulfur Battery Applications. *J. Mater. Chem.* **2011**, *21*, 16603−16610.
(46) Han, S.; Sohn, K.; Hyeon, T. Fabrication of New Nanoporous Carbons through Silica Templates and their Application to the Adsorption of Bulky Dyes. *Chem. Mater.* **2000**, *12*, 3337−3341.
(47) Gierszal, K. P.; Jaroniec, M. Carbons with Extremely Large Volume of Uniform Mesopores Synthesized by Carbonization of Phenolic Resin Film Formed on Colloidal Silica Template. *J. Am. Chem. Soc.* **2006**, *128*, 10026−10027.
(48) Gierszal, K. P.; Jaroniec, M. Large Pore Volume Carbons with Uniform Mesopores and Macropores: Synthesis, Characterization, and Relations between Adsorption Parameters of Silica Templates and Their Inverse Carbon Replicas. *J. Phys. Chem. C* **2007**, *111*, 9742−9748.
(49) Wang, S.; Li, W. C.; Hao, G. P.; Hao, Y.; Sun, Q.; Zhang, X. Q.; Lu, A. H. Temperature-Programmed Precise Control Over the Sizes of Carbon Nanospheres based on Benzoxazine Chemistry. *J. Am. Chem. Soc.* **2011**, *133*, 15304−15307.
(50) Hao, G. P.; Li, W. C.; Qian, D.; Wang, G. H.; Zhang, W. P.; Zhang, T.; Wang, A. Q.; Schüth, F.; Bongard, H. J.; Lu, A. H. Structurally Designed Synthesis of Mechanically Stable Poly(benzoxazine-co-resol)-based Porous Carbon Monoliths and Their Application as High-Performance CO_2 Capture Sorbents. *J. Am. Chem. Soc.* **2011**, *133*, 11378−11388.
(51) Cheng, F.; Wang, S.; Lu, A. H.; Li, W. C. Immobilization of Nanosized $LiFePO_4$ Spheres by 3D Coralloid Carbon Structure with Large Pore Volume and Thin Walls for High Power Lithium-ion Batteries. *J. Power Sources* **2013**, *229*, 249−257.
(52) Knotter, D. M. Etching Mechanism of Vitreous Silicon Dioxide in HF-based Solutions. *J. Am. Chem. Soc.* **2000**, *122*, 4345−4351.
(53) Gonzenbach, U. T.; Studart, A. R.; Tervoort, E.; Gauckler, L. J. Stabilization of Foams with Inorganic Colloidal Particles. *Langmuir* **2006**, *22*, 10983−10988.
(54) Chernyshova, I. V.; Rao, K. H.; Vidyadhar, A.; Shchukarev, A. V. Mechanism of Adsorption of Long-Chain Alkylamines on Silicates: a Spectroscopic Study. 2. Albite. *Langmuir* **2001**, *17*, 775−785.
(55) Wang, J.; Liu, G.; Wang, L.; Li, C.; Xu, J.; Sun, D. Synergistic Stabilization of Emulsions by Poly (oxypropylene) Diamine and Laponite Particles. *Colloid Surface A* **2010**, *353*, 117−124.
(56) Chernyshova, I. V.; Rao, K. H.; Vidyadhar, A.; Shchukarev, A. V. Mechanism of Adsorption of Long-Chain Alkylamines on Silicates. a Spectroscopic Study. 1. Quartz. *Langmuir* **2000**, *16*, 8071−8084.
(57) Vidyadhar, A.; Rao, K. H.; Chernyshova, I. V. Mechanisms of Amine-Feldspar Interaction in the Absence and Presence of Alcohols Studied by Spectroscopic Methods. *Colloid Surf. A* **2003**, *214*, 127−142.

(58) Chmiola, J.; Yushin, G.; Gogotsi, Y.; Portet, C.; Simon, P.; Taberna, P. L. Anomalous Increase in Carbon Capacitance at Pore Sizes Less Than 1 Nanometer. *Science* **2006**, *313*, 1760−1763.
(59) Suss, M. E.; Baumann, T. F.; Worsley, M. A.; Rose, K. A.; Jaramillo, T. F.; Stadermann, M.; Santiago, J. G. Impedance-based Study of Capacitive Porous Carbon Electrodes with Hierarchical and Bimodal Porosity. *J. Power Sources* **2013**, *241*, 266−273.
(60) Zhang, L.; Zhang, G.; Wu, H. B.; Yu, L.; Lou, X. W. Hierarchical Tubular Structures Constructed by Carbon-Coated SnO_2 Nanoplates for Highly Reversible Lithium Storage. *Adv. Mater.* **2013**, *25*, 2589−2593.
(61) Su, F.; Zhao, X. S.; Wang, Y.; Zeng, J.; Zhou, Z.; Lee, J. Y. Synthesis of Graphitic Ordered Macroporous Carbon with a Three-Dimensional Interconnected Pore Structure for Electrochemical Applications. *J. Phys. Chem. B* **2005**, *109*, 20200−20206.
(62) Huang, Y.; Wu, D.; Han, S.; Li, S.; Xiao, L.; Zhang, F.; Feng, X. Assembly of Tin Oxide/Graphene Nanosheets into 3D Hierarchical Frameworks for High-Performance Lithium Storage. *ChemSusChem* **2013**, *6*, 1510−1515.
(63) Lin, J.; Peng, Z.; Xiang, C.; Ruan, G.; Yan, Z.; Natelson, D.; Tour, J. M. Graphene Nanoribbon and Nanostructured SnO_2 Composite Anodes for Lithium Ion Batteries. *ACS Nano* **2013**, *7*, 6001−6006.
(64) Han, F.; Li, W. C.; Li, M. R.; Lu, A. H. Fabrication of Superior-Performance SnO_2@ C Composites for Lithium-Ion Anodes Using Tubular Mesoporous Carbon with Thin Carbon Walls and High Pore Volume. *J. Mater. Chem.* **2012**, *22*, 9645−9651.
(65) Han, F.; Li, D.; Li, W. C.; Lei, C.; Sun, Q.; Lu, A. H. Nanoengineered Polypyrrole-Coated Fe_2O_3@ C Multifunctional Composites with an Improved Cycle Stability as Lithium-Ion Anodes. *Adv. Funct. Mater.* **2013**, *23*, 1692−1700.